2020 IEEE/RSJ International Conference on Intelligent Robots and Systems (IROS)
October 25-29, 2020, Las Vegas, NV, USA (Virtual)

Using Machine Learning for Material Detection with Capacitive Proximity Sensors

Yitao Ding, Hannes Kisner, Tianlin Kong and Ulrike Thomas

***Abstract*— The ability of detecting materials plays an important role in robotic applications. The robot can incorporate the information from contactless material detection and adapt its behavior in how it grasps an object or how it walks on specific surfaces. In this, paper we apply machine learning on impedance spectra from capacitive proximity sensors for material detection. The unique spectra of certain materials only differ slightly and are subject to noise and scaling effects during each measurement. A best-fit classification approach to pre-recorded data is therefore inaccurate. We perform classification on ten different materials and evaluate different classification algorithms ranging from simple k-NN approaches to artificial neural networks, which are able to extract the material specific information from the impedance spectra.**

I. Introduction

The interaction of a robot with the environment relies heavily on the robot's perception. Nowadays, 3D perception technologies provide reliable spatial information for the robot to move within, interact with the surroundings, or manipulate its surroundings. Further sensing modalities widen the perception of the robot and allow reactions optimized to the additional information. One of these extensions is the ability of detecting materials. Despite of having good 3D perception, further material information is beneficial when objects are similar in shape and indistinguishable when using vision alone. This can improve the behavior in how the robot handles and manipulates objects or how it moves in the environment. For example as in Fig. 1, robots with proximity and material sensing on their feet can adapt their motion to the detected surface material. When attached to grippers, the sensors can detect the fill level of a grasped cup or the material of a grasped object. On mobile platforms, such as robotic vacuum cleaners, the information can be used for path optimization or to turn on wiping or suction functions. Material detection with capacitive proximity sensors is in the focus of research, because either the distance to the target or the target's material influences the sensor readings. The knowledge of one of both variables increases the accuracy of the other variable. The use of capacitive sensing modality incorporates several advantages: The measurement requires no probes and is therefore contactless and non-destructive. The measurement is independent to electric isolating surface finishes and can penetrate these layers, such as paint or oxide layers. The electrode design can be adapted to the penetration depth of the measurement. We also gain dual use functionality by having material detection and proximity sensing.

All authors are with the Lab of Robotics and Human-Machine Interaction at Chemnitz University of Technology, Chemnitz, Germany. Emails: {yitao.ding, hannes.kisner, ulrike.thomas}@etit.tu-chemnitz.de

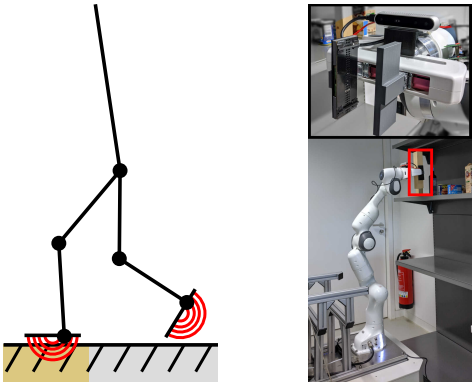

(a) (b)

Fig. 1: Usage scenarios for capacitive material detection: a) A robot with material sensing in its feet. b) A robot sensing materials of grasped objects.

In our previous approach [1], we classify materials based on impedance spectra from capacitive proximity sensors. Originally, the sensors were designed for wide area short range proximity sensing by measuring the capacitive coupling of the electric field at different frequencies to target objects. An additional time-of-flight sensor provides a narrow and far range sensing lobe for absolute distance readings. Therefore, the sensors provide an impedance spectrum which is subject to the material of the target, the distance, and noise from the environment and the sensor itself. The classification method uses 1-Nearest-Neighbor to minimize the error to pre-recorded data. In this paper, we focus on the classification part and extend it with further machine learning algorithms. These range from simple k-nearest-neighbor (k-NN) approaches to artificial neural networks, such as feed forward neural networks (FFNN) and convolutional neural networks (CNN). This paper has two main contributions: First, we apply and evaluate several different machine learning algorithms for material detection with impedance spectra data. Second, we introduce a new classification method by modifying general signal plots of impedance spectra for the use with 2D CNNs for classification.

II. Related Work

As already mentioned, there is an uncertainty in permittivity and distance in capacitive proximity sensing. Therefore, to obtain precise distance measurements, material detection with capacitive proximity sensors was investigated in the past. Kirchner et al. [2] show a model based approach. Based

on the work of Novak et al. [3] and with a further assumption of a frequency dependence permittivity, they first generated training data for three different exciting frequencies at different ranges. The new measurements are then compared to trained data with an error minimization approach for classification. Alagi et al. [4] reduce the uncertainty in distance and permittivity by exploiting the spatial resolution of multiple sensing elements. Similar to triangulation they gain position information of spheric targets of equal dimensions. They first use an artificial neural network to classify different materials with capacitive sensor information.

Besides of material detection with capacitive sensors, numerous approaches have been shown using tactile information [5], [6] where machine learning algorithm play an important role. Xie et al. [7] use high resolution tactile images in combination with sliding motions over different materials and KNNs and SVMs for identification. In [8], [9] the authors generate 3D images based on depth maps from tactile sensor patches. With 3D CNNs they were able to recognize pre-trained objects from which the material information can be reasoned. Chin et al. [10] demonstrate material sorting for recycling with an robotic gripper. They combine strain and capacitive sensors on the finger and use stiffness and electric-field measurements as classifier.

In the field of electrical impedance spectroscopy with contacting probes, Guermazi et. al [11] demonstrated successfully approaches for meat quality inspection. Helwan et. al [12] showed promising results for breast cancer detection through impedance spectroscopy with neural networks.

III. Sensing

In order to obtain the impedance spectrum, we measure the electrode current and electrode voltage of the capacitive sensor at different exciting frequencies.

A. Sensor Design

The sensor (Fig. 2) is a refined design of our previous sensor [1]. As shown in Fig. 3 the capacitive coupling of the sensor's electrode to the target is measured with an AC exciting signal generated from a direct digital synthesizer (DDS). ADC1 measures the exciting signal u_1 while ADC2 measures the signal u_2 after the measurement resistor R_m which is also the electrode signal.

The sensor has a differential design [13] in which the second grounding electrode is driven with a differential signal instead. This method allows measurements which are unaffected by the grounding state of the target object. Besides at further distances electrical interferences to other devices are reduced.

In this work, the amplitude $\hat{u}_1$ of the exciting signal u_1 is around $\pm 2.5\,\mathrm{V}$ and R_m is set to $47\,\mathrm{k\Omega}$. The sampling rate of each ADC is $9\,\mathrm{MHz}$ with a sampling window of up to 4096 samples for each impedance measurement.

B. Electrode Design

The design of the electrodes greatly influences the results of material recognition. Given that the overall electrode area

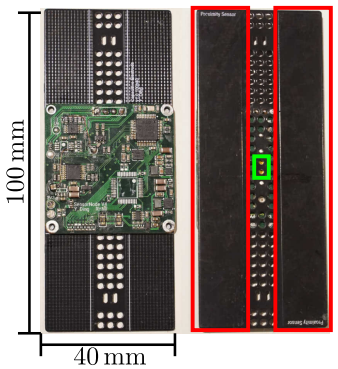

Fig. 2: Capacitive proximity sensor with time-of-flight sensing module (green). The capacitive electrodes are marked in red.

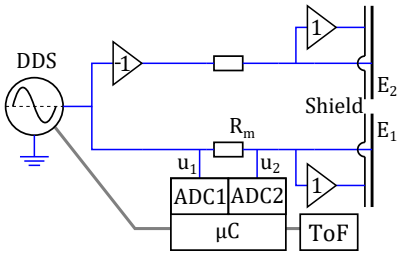

Fig. 3: Simplified sensor diagram.

is limited, an optimal ratio of electrode size and spacing must be found. It is desirable to have strong capacitive coupling to the target object and no parasitic capacitance. Parasitic capacitances add offsets to the signal, which minimizes the dynamic range during data acquisition. In Fig. 4, finite element method (FEM) simulations of the electric flux density with different electrode spacing and fixed target distance are shown. The cross section view in Fig. 4a shows that close electrodes create strong coupling to the target since the electrode area is larger. On the other hand, the parasitic coupling between both electrodes increases. With wide spacing (Fig. 4c) the electric field lines go through the target object. However, because of the weaker capacitive coupling the measured signal is prone to noise. We select the spacing to be the same size as the electrodes (Fig. 4b) which provides a good trade-off between noise immunity and dynamic range. Close electrode distances in combination with a comb structure (more gaps) generate their main electric fields close to the electrodes and cancel out each other at further distances. The effect can be exploited to measure specifically close to the surface of a target since the electric fields do not penetrate the object in the deeper areas. Furthermore, the sensitivity can be tuned for different measurement distances.

C. Impedance Spectrum

In order to obtain the impedance spectrum the DDS generates a frequency sweep from $20\,\mathrm{kHz}$ to $1000\,\mathrm{kHz}$ with a resolution of $1\,\mathrm{kHz}$. With each frequency step increase, the electrode impedance Z is calculated which requires the knowledge of the amplitude of the exciting signal $\hat{u}_1$, the signal amplitude at the electrode $\hat{u}_2$, and the phase between

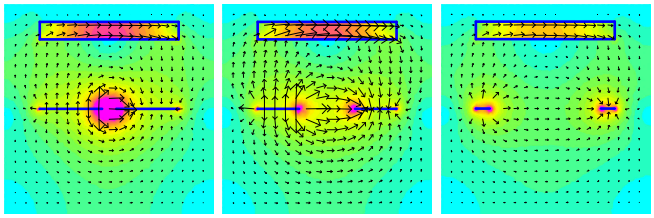

(a) 1. (b) 2. (c) 3.

Fig. 4: Cross section view of electrodes and target. FEM simulation of electric flux density between electrodes with different spacings.

both signals φ. Let u be an ac signal with known frequency f and unknown amplitude $\hat{u}$ and phase φ:

$$u = \hat{u} \cos\left(2\pi f t + \varphi\right). \tag{1}$$

We can exploit the knowledge of f and calculate the amplitude with the inner product of the time series vector u.

$$\hat{u} = \sqrt{2\left\langle u, u \right\rangle} \tag{2}$$

Compared to performing discrete Fourier transform (DFT) this method reduces the computational effort by avoiding the calculations of the reference in-phase and quadrature values. Noise caused by missmatch and jitter in the frequency can also be compensated. The phase φ between u_1 and u_2 can be calculated as follows:

$$\varphi = \pm \arccos\left(\frac{2}{\hat{u}_1 \hat{u}_2}\left\langle u_1, u_2 \right\rangle\right). \tag{3}$$

Note: φ is negative since capacitances are measured. The impedance at the electrodes Z is:

$$Z = R_\mathrm{m}\left(\frac{\hat{u}_2 e^{-j\varphi}}{\hat{u}_1 - \hat{u}_2 e^{j\varphi}}\right) \tag{4}$$

In order to compensate the large influence of the frequency to the impedance, the capacitance C at the electrode is calculated.

$$C = \frac{1}{j2\pi f Z} \tag{5}$$

IV. Material Classification

In this work we perform classification on ten materials as listed in Table I. Each material has 200 capacitance spectra recorded at different positions of different samples. Furthermore, noise from sliding motion is intentionally introduced into the measurements to reproduce motions of the final application (e.g. robotic feet, robot vacuum, or motion during grasping with a gripper). The frequency sweeps from 20 kHz to 1000 kHz generates 2×980 data points which are split into real and imaginary values for each spectrum acquisition. Depending on the final algorithm, the data is used either as a single feature vector or kept seperated as two individual vectors.

Label	Material
0	Air
1	Aluminium
2	Cement
3	Glass
4	PVC
5	Steel
6	Rock
7	Ceramic
8	Water
9	Wood

TABLE I: Table of materials for classification.

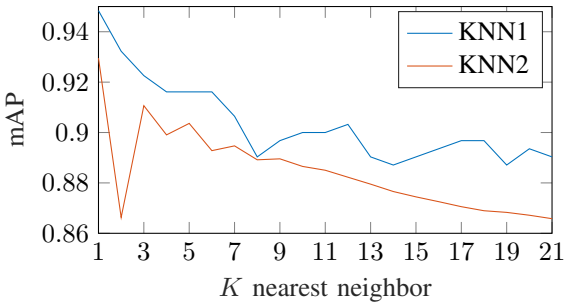

Fig. 5: mAP vs. k nearest neighbors. Low k value provides best results.

A. k-Nearest Neighbor Classification

With k-NN one can search for each impedance value in the measured spectrum k nearest neighbors from the training dataset. The class with most correspondences is the final classification result.

For the first variant *KNN1*, we set $k = 1$ and perform classification on the capacitance spectrum. We also implemented a frequency-wise nearest neighbor classification with $k = 1$ with *KNN2*. The k value was chosen according to Fig. 5, where we tested different k values for the mean average precision (mAP). *KNN2* picks its nearest neighbors for each frequency instead within the complete spectrum. The final result is the classifier with most similarities. The idea behind this setting is that the material information between different frequencies are only weakly linked. Therefore a complete search within the spectra as in *KNN1* may lead to false matches. Due to its simplicity and low computational effort, k-NN only requires memory for storing the training dataset and can be implemented in microcontrollers to provide in-sensor classification functionalities.

B. Feed Forward Neural Network

Neural networks provide mapping functions that predict output values for certain input values. The mapping functions has to be learned with training data. The structure of the network influences the network performance and relates also to the complexity of the trainable mapping function. Often complex structures can learn complex classification functions. Our classification task is comparatively easy. A very simple k-NN-approach is capable to perform the classification task with high accuracies. Thus, our networks use few hidden layers to achieve small complexity as well as being able to perform similarly to k-NN approaches while being more robust to noisy input data.

The feed forward neural networks for material classification are illustrated in Fig. 6. We use three different versions with differences in neuron count and activation function. The input layer accepts a single feature vector with $2N$ length for the real and imaginary parts of the impedance spectrum which corresponds to 2×980 inputs. The input data is normalized to the maximum and minimum value of the dataset.

The training optimizer updates the weight parameter of the layer during training to minimize a loss function. We use the state-of-the-art Adam optimizer [14] with no learning rate changes to maintain the simplicity of the overall classification task. Furthermore, we use the categorical cross-entropy as the loss-function for our multiclass classification. Therefore, our last layer uses the softmax function which performs well with the log in the loss function. The hidden layers use the common sigmoid activation functions.

ANN1 is a standard network with 1536, 1024, and 512 neurons in the hidden layers one to three respectively. We chose the number of input layer in terms of the number of features available and the output classes. We have 1,536 input features, which is almost equal to our input vector. The next neurons per layer are given by gradually reducing their number to the number of output classes. The sigmoid function is used as activation function. Compared to *ANN1*, *ANN2* applies the rectified linear unit function (ReLU) as activation function and *ANN3* has fewer neurons (384, 256, 128).

We also reduced the input vector size (number of frequencies) to 2×300 to investigate a second set of networks and labeled them as *ANNx**R***. The reduction is performed through meaning and summarizing multiple frequencies which reduces noise, but may also reduce material specific properties in the spectra.

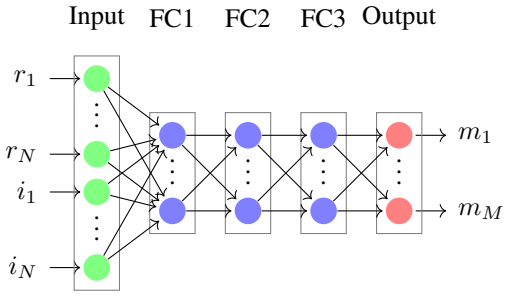

Fig. 6: FFNN with $2N$ inputs for real and imaginary values of the spectrum and $M = 10$ outputs.

C. Convolutional Neural Network

Classification of 1D signals can be realized with 1D-CNNs or by converting the signal into a 2D image for 2D-CNNs. Often these signals are in time series or frequency series, where a specific pattern has to be recognized. 1D-CNNs reduce the computational complexity of CNNs into one dimension. Thus, real-time applications can be implemented with cheaper and simpler hardware configurations [15]. Hatami et al. [16] convert 1D time series signals to 2D images and use a custom 2D-CNN for classification. In our approach, we first evaluate 1D-CNNs, which is configured as in Fig. 7. The input layer accepts two individual feature vectors for real and imaginary parts of the spectrum. The 1D convolution layers are divided in three groups, where the first and last group have 100 neurons each and the second group 256 neurons for each layer.

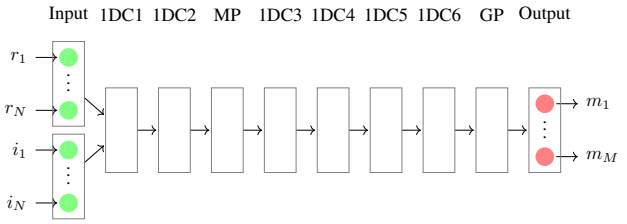

Fig. 7: 1DCNN with 1D convolutional layers (1DC), max pooling layer (MP), and global average pooling (GP) layer.

In the last approach, we investigate the performance of 2D-CNNs for material detection which are mainly used for image recognition. During our early work we noticed, that humans are actually able to classify some materials based on the impedance spectra plots. Therefore, we convert the plots to images and use available CNNs (*InceptionV3* [17] and *ResNet18* [18]) for image recognition. In our case, the impedance spectra are composed of two 1D signals of real and imaginary signals. The 2D conversion has to incorporate both signals into a single image while keeping scaling information. The absolute values of the spectra is lost due to the scaling of the plot to fit exactly within the image size of 299×299 pixels. The image size is the maximum size for the InceptionV3 network. Recent CNN applications resize large image sizes to fit the resolution of the used backbone network. However, due to image preprocessing and image encoding the pixel may not represent the correct data. Thus, we perform a filter step before generating the images. We encode the scaling information in the color spectrum as shown in Fig. 9. The real part of the spectra is plotted in the red channel and the imaginary part in the blue channel. To encode the scaling value, the brightness of each color channel is used. Here the maximum brightness of the channel represents the maximum value in the dataset, while the minimum brightness stands for the minimum value in the dataset. The green channel represents the shape of the curve and is always on full brightness. A further dataset is generated with a horizontal line (labeled with an additional *L*) with its vertical position representing the mean value of the spectra normalized to the maximum and minimum dataset values.

V. Experimental Results

For the performance evaluation of the classification algorithms, 70 % of the dataset (Fig. 10) are randomly selected as training data for each label, while the rest is equally split to evaluation and test data. The precision-recall curve provides a general quality value of the algorithms. Note that the precision-recall curve for *KNN1* does not exist, since

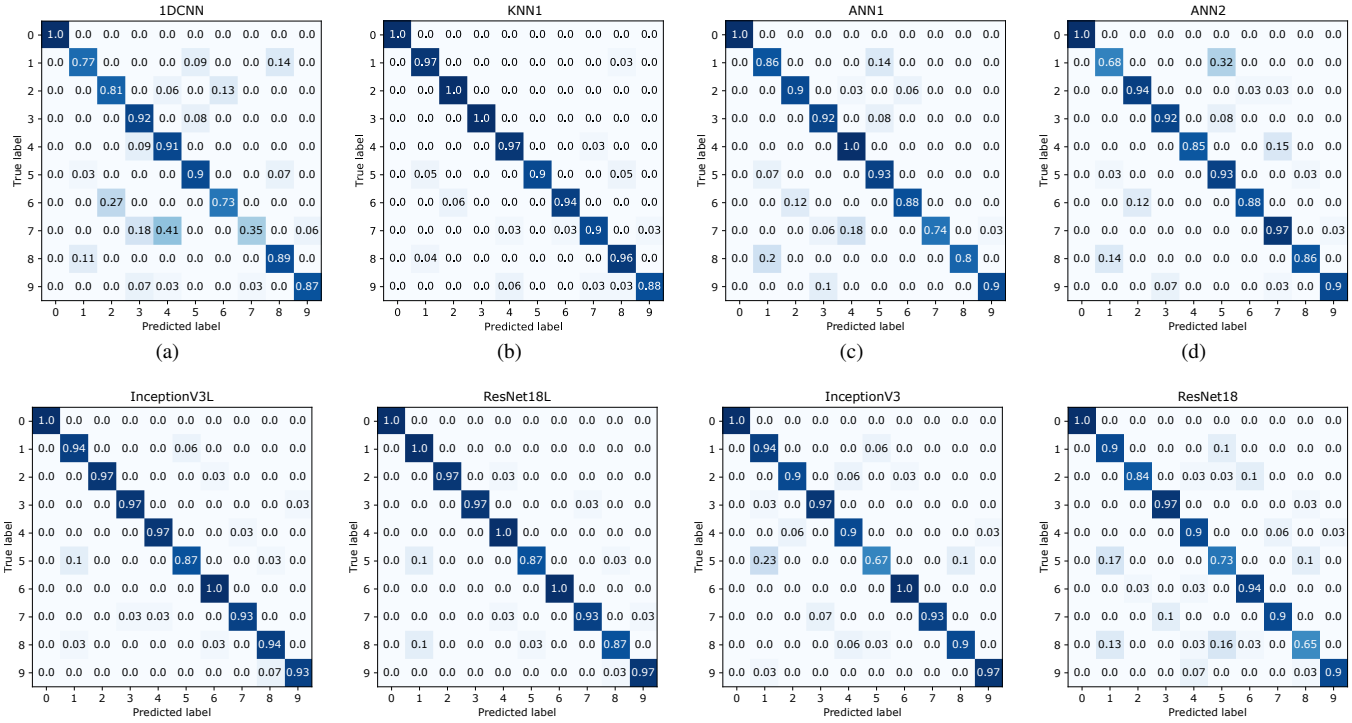

Fig. 8: Confusion matrix of all well performing algorithms and 1DCNN as underperforming reference. The labels are listed in Tab. I.

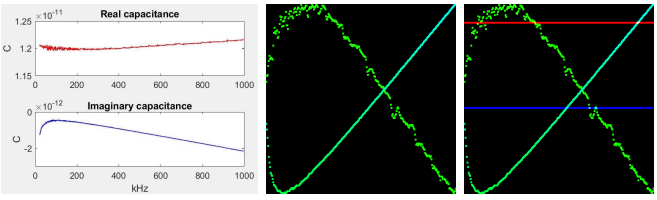

Fig. 9: Conversion of impedance spectrum (capacitance vs. frequency) plots (Fig. 9a) to images (Fig. 9b, 9c) for classification with image based CNNs.

the algorithm only outputs the most similar class without precision values. On the other hand, since *KNN2* classifies frequency-wise, a precision value can be calculated from the ratio of classification outputs from each frequency. The first curve Fig. 11a shows the mean precision-recall curve of all well performing algorithms (mAP > 0.95), while all underperforming algorithms are listed in the second plot Fig. 11b. Here, the algorithms with reduced input data *ANNxR* show poor performance, as well as *ANN3*. The result indicates insufficient numbers of neurons in the networks, since these networks have reduced numbers of neurons either in the input layer *ANNxR* or hidden layers *ANN3*. This is especially supported by the significant under performance in the precision-recall curve of *ANN3R*, where the neural network has reduced neuron counts in both the input layer and the hidden layers. The results of *ANN1* and *ANN2* are similar. Thus showing that small changes in the network structure, e.g. the sigmoid and the ReLU activation function, lead to small differences in the performance. Moreover, this shows the robustness of the network structure.

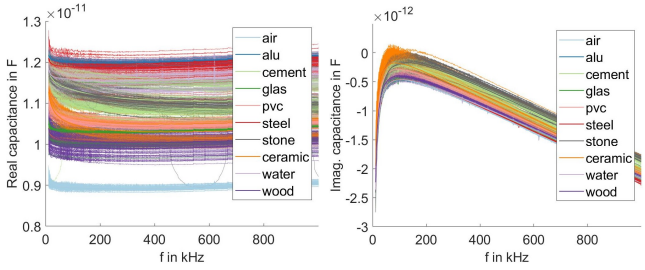

Fig. 10: Capacitance measurements of all materials with large variance among the samples.

In the well performing group, the image recognition networks show exceptionally good performance compared to the standard neural networks *ANN1* and *ANN2*. A look at the confusion matrices of these algorithms Fig. 8 reveals that certain materials, such as aluminium (label 1), steel (label 5), and water (label 8) are difficult to differentiate because of their similar conductivity properties. Here, the image recognition based methods outperform the 1D algorithms. Especially, the *InceptionV3L* and *ResNet18L* with their additional added horizontal lines in the images provide good results. *KNN1* delivers unexpected good results for its

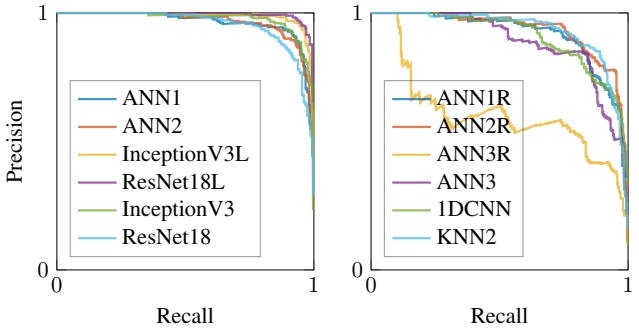

(a) (b)

Fig. 11: Mean precision-recall curve of good performing a) (mAP > 0.95) and underperforming b) networks.

simple algorithm and is comparable to *ANN1* and *ANN2*. The robustness of these *InceptionV3L* and *ResNet18L* should be highlighted, as a high percentage of measurements are noisy due to sliding motions during data acquisition as shown in Fig. 12. Overall, the results in this work are outperforming

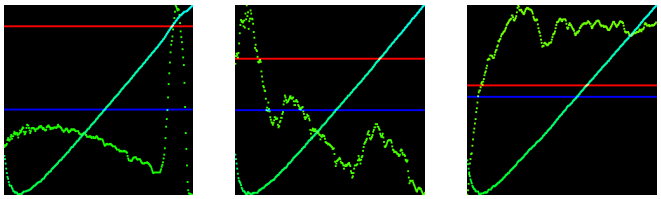

(a) (b) (c)

Fig. 12: Images for CNNs: Noisy measurements due to motion during data acquisition.

existing works based on tactile data [7], [19] which indicate a higher material information content in capacitive measurements.

VI. Conclusion

In this paper, we evaluate different machine learning algorithms for material identification for sensor signals from capacitive proximity sensors. The conclusion of this paper is that simple machine learning algorithms provide good results for this task. Especially when converting the 1D spectra data to images, image based CNNs are able to identify materials that are very similar in their electrical properties. In applications, where fine granular identification is unnecessary, standard FFNNs or k-NN algorithms provide reasonable results. Therefore, these algorithms can be implemented within the sensing hardware, since k-NN only requires low computational effort and storage for the training dataset. The detection is also very robust against noise generated by sliding motions during data acquisition. Therefore, this sensing method can be used for the presented applications (robotic feet, grasping, and robotic vacuum cleaner) where motion is always present. A major drawback of machine learning algorithms compared to model based approaches exists when system conditions vary. A change in electrode design or circuit parameters requires new training datasets, which is time-consuming to create.

References

[1] Y. Ding, H. Zhang, and U. Thomas, "Capacitive proximity sensor skin for contactless material detection," in *2018 IEEE/RSJ International Conference on Intelligent Robots and Systems (IROS)*, Oct 2018, pp. 7179–7184.

[2] N. Kirchner, D. Hordern, D. Liu, and G. Dissanayake, "Capacitive sensor for object ranging and material type identification," *Sensors and Actuators A: Physical*, vol. 148, no. 1, pp. 96 – 104, 2008.

[3] J. L. Novak and J. J. Wiczer, "A high-resolution capacitative imaging sensor for manufacturing applications," in *1991 IEEE International Conference on Robotics and Automation*, April 1991, pp. 2071–2078 vol.3.

[4] H. Alagi, A. Heilig, S. E. Navarro, T. Kroeger, and B. Hein, "Material recognition using a capacitive proximity sensor with flexible spatial resolution," in *2018 IEEE/RSJ International Conference on Intelligent Robots and Systems (IROS)*, Oct 2018, pp. 6284–6290.

[5] M. Kaboli, D. Feng, and G. Cheng, "Active tactile transfer learning for object discrimination in an unstructured environment using multimodal robotic skin," *International Journal of Humanoid Robotics*, vol. 15, no. 01, p. 1850001, 2018.

[6] S. Ottenhaus, L. Kaul, N. Vahrenkamp, and T. Asfour, "Active tactile exploration based on cost-aware information gain maximization," *International Journal of Humanoid Robotics*, vol. 15, no. 01, p. 1850015, 2018.

[7] Y. Xie, C. Chen, D. Wu, W. Xi, and H. Liu, "Human-touch-inspired material recognition for robotic tactile sensing," *Applied Sciences*, vol. 9, no. 12, 2019.

[8] F. Pastor, J. M. Gandarias, A. J. García-Cerezo, and J. M. Gómez-de Gabriel, "Using 3d convolutional neural networks for tactile object recognition with robotic palpation," *Sensors*, vol. 19, no. 24, 2019.

[9] J. M. Gandarias, A. J. García-Cerezo, and J. M. Gómez-de-Gabriel, "Cnn-based methods for object recognition with high-resolution tactile sensors," *IEEE Sensors Journal*, vol. 19, no. 16, pp. 6872–6882, Aug 2019.

[10] L. Chin, J. Lipton, M. C. Yuen, R. Kramer-Bottiglio, and D. Rus, "Automated recycling separation enabled by soft robotic material classification," in *2019 2nd IEEE International Conference on Soft Robotics (RoboSoft)*, April 2019, pp. 102–107.

[11] M. Guermazi, O. Kanoun, and N. Derbel, "Investigation of long time beef and veal meat behavior by bioimpedance spectroscopy for meat monitoring," *IEEE Sensors Journal*, vol. 14, no. 10, pp. 3624–3630, Oct 2014.

[12] A. Helwan, J. B. Idoko, and R. H. Abiyev, "Machine learning techniques for classification of breast tissue," *Procedia Computer Science*, vol. 120, pp. 402 – 410, 2017, 9th International Conference on Theory and Application of Soft Computing, Computing with Words and Perception.

[13] Y. Ding and U. Thomas, "A new capacitive proximity sensor for detecting ground-isolated objects," in *Proceedings of the 1st Workshop on Proximity Perception in Robotics at IROS 2018, Madrid, Spain*, Aug 2018, pp. 7–8.

[14] D. P. Kingma and J. Ba, "Adam: A method for stochastic optimization," 2014.

[15] S. Kiranyaz, T. Ince, and M. Gabbouj, "Real-time patient-specific ecg classification by 1-d convolutional neural networks," *IEEE Transactions on Biomedical Engineering*, vol. 63, no. 3, pp. 664–675, March 2016.

[16] N. Hatami, Y. Gavet, and J. Debayle, "Classification of time-series images using deep convolutional neural networks," *CoRR*, vol. abs/1710.00886, 2017.

[17] C. Szegedy, V. Vanhoucke, S. Ioffe, J. Shlens, and Z. Wojna, "Rethinking the inception architecture for computer vision," *CoRR*, vol. abs/1512.00567, 2015.

[18] K. He, X. Zhang, S. Ren, and J. Sun, "Deep residual learning for image recognition," in *2016 IEEE Conference on Computer Vision and Pattern Recognition (CVPR)*, June 2016, pp. 770–778.

[19] A. Murali, Y. Li, D. Gandhi, and A. Gupta, "Learning to grasp without seeing," *CoRR*, vol. abs/1805.04201, 2018. [Online]. Available: http://arxiv.org/abs/1805.04201